13th International Conference on Applications of Statistics and Probability in Civil Engineering, ICASP13
Seoul, South Korea, May 26-30, 2019

Uncertainty Propagation Analysis in Stochastic Structural Dynamics: A Parametric Substructure Approach

Hector Jensen
Professor, Dept. of Civil Engineering, Federico Santa Maria University, Valparaiso, Chile, Dept. of Civil Engineering, Tongji University, Shanghai, China

Franco Mayorga
Research Engineer, Dept. of Civil Engineering, Federico Santa Maria University, Valparaiso, Chile

Claudio Larenas
Undergraduate Student, Dept. of Civil Engineering, Federico Santa Maria University, Valparaiso, Chile

Jianbing Chen
Professor, Dept. of Civil Engineering, Tongji University, Shanghai, China

ABSTRACT: A physical domain-based formulation of parametric reduced-order models based on dominant normal modes and interface reduction is presented in the context of uncertainty propagation analysis. Normal and interface modes are approximated in terms of a set of support points in the uncertain parameter space. Based on these approximate modes, reduced-order matrices can be updated efficiently during the simulation process associated with the uncertainty analysis. The proposed approach is applied to a complex nonlinear finite element model under a synthetic ground motion generated by a realistic source-based model for subduction mega-thrust earthquakes.

1. INTRODUCTION

It is often impractical to carry out a finite element analysis of the full structure in cases of complex and large systems. In this framework, the so-called Craig-Bampton method has been developed as a practical and efficient tool for modeling and analyzing the dynamics of complex structural systems (Craig (1981)). The basic idea of the technique is to describe the dynamic behavior of a structure by a set of normal modes of individual substructures plus a set of static vectors that account for the coupling at each interface where the substructures are connected. In this manner, each substructure is dynamically reduced by a separate modal analysis before being assembled at the system level. As a result, a reduced-order model of the entire structure is obtained. In the approach, the normal modes correspond to the dominant fixed interface modes while the attachment at the interfaces is achieved by a set of interface constraint modes. Although an important order reduction may be achieved for the individual substructures there is no order reduction for the interface. To reduce the number of interface degrees of freedom, a number of approaches have been proposed in the literature. In particular, a method based on characteristic constraint modes has proved to be computationally quite attractive (Castanier et al. (2001)). In the context of uncertainty analysis, the construction of reduced-order models at each sample point, implies re-computing the fixed-interface and constraint normal modes for each substructure as well

as the interface modes. This procedure can be computationally very expensive due to the substantial computational overhead that arises at substructure level (Papadimitriou and Papadioti (2013)). To cope with this difficulty, an efficient finite element model parametrization scheme is presented.

2. REDUCED-ORDER MODEL

2.1. Mechanical modeling

A general class of nonlinear structural dynamical systems can be characterized by a multi-degree-of-freedom model satisfying the equation of motion

$$\begin{aligned}\mathbf{M}\ddot{\mathbf{x}}(t) + \mathbf{C}\dot{\mathbf{x}}(t) + \mathbf{K}\mathbf{x}(t) = \\ \mathbf{f}_{NL}(\mathbf{x}(t),\dot{\mathbf{x}}(t),\mathbf{y}(t)) + \mathbf{f}(t)\end{aligned} \tag{1}$$

where $\mathbf{x}(t)$ denotes the displacement vector of dimension n, $\mathbf{f}_{NL}(\mathbf{x}(t),\dot{\mathbf{x}}(t),\mathbf{y}(t))$ the vector of nonlinear restoring forces, $\mathbf{y}(t)$ the vector of a set of variables which describes the state of the nonlinear components, and $\mathbf{f}(t)$ the external force vector. The matrices $\mathbf{M}$, $\mathbf{C}$, and $\mathbf{K}$ describe the mass, damping, and stiffness, respectively. The evolution of the set of variables $\mathbf{y}(t)$ is described by an appropriate nonlinear model which depends on the nature of the nonlinearity. The equation of motion for the displacement vector $\mathbf{x}(t)$ and the equation for the evolution of the set of variables $\mathbf{y}(t)$ constitute a system of coupled non-linear equations.

2.2. Reduced-order matrices based on dominant normal modes

To define the reduced-order model, the so-called dominant fixed interface normal modes $\mathbf{\Phi}^s_{id}$ and interface constraint modes $\mathbf{\Psi}^s_{ib}$ for each substructure $s, s = 1,...,N_s$ are considered (Craig (1981)). Based on these modes, the mass and stiffness matrices referred to the vector of dominant fixed-interface modal coordinates of all substructures and to the vector of physical coordinates at the independent interfaces take the form (Jensen et al. (2017))

$$\begin{aligned}\hat{\mathbf{M}}_R &= \begin{bmatrix} [\mathbf{I},..,\mathbf{I}] & \mathbf{M}_{ib\Gamma} \\ \mathbf{M}^T_{ib\Gamma} & \mathbf{M}_\Gamma \end{bmatrix} \\ \hat{\mathbf{K}}_R &= \begin{bmatrix} [\mathbf{\Lambda}^1_{id},..,\mathbf{\Lambda}^{N_s}_{id}] & \mathbf{0} \\ \mathbf{0} & \mathbf{K}_\Gamma \end{bmatrix}\end{aligned} \tag{2}$$

where

$$\begin{aligned}\mathbf{M}_\Gamma &= \tilde{\mathbf{T}}^T[\hat{\mathbf{M}}^1_{bb},...,\hat{\mathbf{M}}^{N_s}_{bb}]\tilde{\mathbf{T}} \\ \mathbf{K}_\Gamma &= \tilde{\mathbf{T}}^T[\hat{\mathbf{K}}^1_{bb},...,\hat{\mathbf{K}}^{N_s}_{bb}]\tilde{\mathbf{T}} \\ \mathbf{M}_{ib\Gamma} &= [\hat{\mathbf{M}}^1_{ib},...,\hat{\mathbf{M}}^{N_s}_{ib}]\tilde{\mathbf{T}} \\ \hat{\mathbf{M}}^s_{ib} &= \mathbf{\Phi}^{s^T}_{id}\mathbf{M}^s_{ii}\mathbf{\Psi}^s_{ib} + \mathbf{\Phi}^{s^T}_{id}\mathbf{M}^s_{ib}, s = 1,...,N_s \\ \hat{\mathbf{K}}^s_{bb} &= \mathbf{K}^{s^T}_{ib}\mathbf{\Psi}^s_{ib} + \mathbf{K}^s_{bb} \\ \hat{\mathbf{M}}^s_{bb} &= (\mathbf{\Psi}^{s^T}_{ib}\mathbf{M}^s_{bb} + \mathbf{M}^{s^T}_{ib})\mathbf{\Psi}^s_{ib} + \mathbf{\Psi}^{s^T}_{ib}\mathbf{M}^s_{ib} + \mathbf{M}^s_{bb}\end{aligned} \tag{3}$$

and where the subscript T denotes the transpose of a matrix. The diagonal matrices $\mathbf{\Lambda}^s_{id}, s = 1,...,N_s$ contain the n^s_{id} kept eigenvalues associated with the fixed-interface normal modes for each substructure (dominant fixed interface normal modes). Additional matrices involved in the definition of $\hat{\mathbf{M}}_R$ and $\hat{\mathbf{K}}_R$ include the partition matrices of the mass and stiffness matrices at substructure level and a transformation matrix $\tilde{\mathbf{T}}$. This matrix maps the vector of physical coordinates at the independent interfaces to the vector of interface coordinates of all substructures (Jensen et al. (2017)). The dimension of the matrices $\hat{\mathbf{M}}_R$ and $\hat{\mathbf{K}}_R$ is equal to $n_R \times n_R$, where $n_R = \sum_{s=1}^{N_s} n^s_{id} + n_\Gamma$, being n_Γ the total number of degrees of freedom at the independent interfaces.

2.3. Reduced-order matrices based on interface reduction

As previously pointed out, a method based on characteristic constraint modes is considered for interface reduction. The approach corresponds to an eigenvalue problem of the interface constraint mode partitions of the reduced-order matrices (Castanier et al. (2001)), that is

$$\mathbf{K}_\Gamma\mathbf{\Upsilon}_I - \mathbf{M}_\Gamma\mathbf{\Upsilon}_I\mathbf{\Omega}_I = \mathbf{0} \tag{4}$$

The matrix $\mathbf{\Upsilon}_I$ contains the selected n_I interface modes and $\mathbf{\Omega}_I$ is the diagonal matrix that contains the corresponding eigenvalues. The interface modes correspond to the so-called characteristic constraint modes at the interface level. The kept set of interface modes is used to represent the vector of physical coordinates at the independent interfaces $\mathbf{x}_\Gamma(t)$, as $\mathbf{x}_\Gamma(t) = \mathbf{\Upsilon}_I\boldsymbol{\eta}_I(t)$, where $\boldsymbol{\eta}_I(t)$

are the interface modal coordinates. Using this representation, the corresponding reduced mass matrix $\hat{\mathbf{M}}_{RI} \in \mathbb{R}^{n_{RI} \times n_{RI}}$ and reduced stiffness matrix $\hat{\mathbf{K}}_{RI} \in \mathbb{R}^{n_{RI} \times n_{RI}}, n_{RI} = \sum_{s=1}^{N_s} n_{id}^s + n_I$ are given by (Jensen et al. (2017))

$$\hat{\mathbf{M}}_{RI} = \begin{bmatrix} [\mathbf{I}, ..., \mathbf{I}] & \mathbf{M}_{ib\Gamma}\boldsymbol{\Upsilon}_I \\ \boldsymbol{\Upsilon}_I^T \mathbf{M}_{ib\Gamma}^T & \mathbf{I}_I \end{bmatrix} \qquad (5)$$
$$\hat{\mathbf{K}}_{RI} = \begin{bmatrix} [\boldsymbol{\Lambda}_{id}^1, ..., \boldsymbol{\Lambda}_{id}^{N_s}] & \mathbf{0} \\ \mathbf{0} & \boldsymbol{\Omega}_I \end{bmatrix}$$

The dimension of the reduced order matrices can be significantly smaller than the dimension of the unreduced matrices, i.e. $n_{RI} \ll n$.

3. PARAMETRIZATION OF REDUCED-ORDER MODELS

3.1. Parametrization of substructure matrices

In the context of uncertainty propagation analysis, it is assumed that the finite element model is parametrized by a set of parameters $\boldsymbol{\theta} \in \Omega_{\boldsymbol{\theta}} \subset R^{n_\theta}$. Such parameters are characterized by a joint probability density function $q(\boldsymbol{\theta})$. It is also assumed that the mass and stiffness matrices of each substructure allow the expansion

$$\mathbf{M}^s(\boldsymbol{\theta}) = \sum_{j=1}^{N_{sg}} \bar{\mathbf{M}}^{sj} g_j(\boldsymbol{\theta}), \mathbf{K}^s(\boldsymbol{\theta}) = \sum_{j=1}^{N_{sh}} \bar{\mathbf{K}}^{sj} h_j(\boldsymbol{\theta}) \qquad (6)$$

where N_{sg} and N_{sh} are the number of parametrization functions $g_j(\cdot)$ and $h_j(\cdot)$ related to the substructure s, respectively, and the matrices $\bar{\mathbf{M}}^{sj}$ and $\bar{\mathbf{K}}^{sj}$ are independent of the model parameters $\boldsymbol{\theta}$. It is noted that the previous expansions are usually encountered in structural systems modeled by standard finite elements, where the model parameters could be geometric or material properties.

3.2. Parametrization of interface constraint modes

To approximate the interface constraint modes at a new sample point $\boldsymbol{\theta}^k$, generated during the simulation process associated with the uncertainty analysis, it is assumed that $\boldsymbol{\Psi}_{ib}^s(\boldsymbol{\theta})$ have been evaluated at L support points in the model parameters space, i.e., $\boldsymbol{\theta}^l, l = 1, ...L$. In addition, the modes for a nominal point $\boldsymbol{\theta}^0$ have also been computed. The nominal point may correspond to the reference model or it can be chosen as the mean value of the uncertain model parameters. Based on this information, the interface constraint modes evaluated at $\boldsymbol{\theta}^k$ are approximated by means of a linear interpolation as (Goller et al. (2011))

$$\boldsymbol{\Psi}_{ib}^s(\boldsymbol{\theta}^k) = (1 - \sum_{l=1}^{L} \xi_l^k)\boldsymbol{\Psi}_{ib}^s(\boldsymbol{\theta}^0) + \sum_{l=1}^{L} \xi_l^k \boldsymbol{\Psi}_{ib}^s(\boldsymbol{\theta}^l) \qquad (7)$$

where the coefficient ξ_l^k represents the contribution of the support point $\boldsymbol{\theta}^l$ to the simulation point $\boldsymbol{\theta}^k$. To consider only interpolations, the simulation point $\boldsymbol{\theta}^k$ should belong to the n_θ-dimensional convex hull of the support points (Seidel (1997)). The determination of the interpolation coefficients is discussed in a subsequent Section.

3.3. Parametrization of dominant fixed-interface modes

To approximate the fixed-interface normal modes, they are first written as in Eq. (7), that is,

$$\hat{\boldsymbol{\Phi}}_{id}^s(\boldsymbol{\theta}^k) = (1 - \sum_{l=1}^{L} \xi_l^k)\boldsymbol{\Phi}_{id}^s(\boldsymbol{\theta}^0) + \sum_{l=1}^{L} \xi_l^k \boldsymbol{\Phi}_{id}^s(\boldsymbol{\theta}^l) \qquad (8)$$

where the interpolation coefficients ξ_l^k, $l = 1, ..., L$ are the ones introduced in Eq. (7). Note that in this case, the dominant fixed-interface modes need to be computed at the support points $\boldsymbol{\theta}^l$, $l = 1, ..., L$ and at the nominal point $\boldsymbol{\theta}^0$, i.e. $\boldsymbol{\Phi}_{id}^s(\boldsymbol{\theta}^l), l = 0, 1, ..., L$. The previous interpolation expression is not used directly since the approximate dominant fixed-interface normal modes are not calculated directly from the solution of an eigenvalue problem. Instead, they are used as a subspace to span the dominant fixed-interface normal modes. In other words, the actual approximate eigenvectors $\boldsymbol{\Phi}_{id}^s(\boldsymbol{\theta}^k)$ are defined as linear combination of the vectors composing the matrix $\hat{\boldsymbol{\Phi}}_{id}^s(\boldsymbol{\theta}^k)$, that is, $\boldsymbol{\Phi}_{id}^s(\boldsymbol{\theta}^k) = \hat{\boldsymbol{\Phi}}_{id}^s(\boldsymbol{\theta}^k)\mathbf{Q}(\boldsymbol{\theta}^k)$, where $\mathbf{Q}(\boldsymbol{\theta}^k)$ is an auxiliary matrix. It can be shown that $\mathbf{Q}(\boldsymbol{\theta}^k)$ can be obtained from the solution of the reduced eigenproblem (Mayorga and Jensen (2018))

$$\left[\hat{\boldsymbol{\Phi}}_{id}^{s^T}(\boldsymbol{\theta}^k)\mathbf{K}_{ii}^s(\boldsymbol{\theta}^k)\hat{\boldsymbol{\Phi}}_{id}^s(\boldsymbol{\theta}^k)\right]\mathbf{Q}(\boldsymbol{\theta}^k) = \left[\hat{\boldsymbol{\Phi}}_{id}^{s^T}(\boldsymbol{\theta}^k)\mathbf{M}_{ii}^s(\boldsymbol{\theta}^k)\hat{\boldsymbol{\Phi}}_{id}^s(\boldsymbol{\theta}^k)\right]\mathbf{Q}(\boldsymbol{\theta}^k)\boldsymbol{\Omega}(\boldsymbol{\theta}^k) \tag{9}$$

where the matrices inside the brackets are of dimension $n_{id}^s \times n_{id}^s$. The previous information provides an approximation for the dominant fixed-interface normal modes at the sample point $\boldsymbol{\theta}^k$, and for the corresponding eigenvalues, i.e., $\boldsymbol{\Lambda}_{id}^s(\boldsymbol{\theta}^k) = \boldsymbol{\Omega}(\boldsymbol{\theta}^k)$.

3.4. Parametrization of interface modes

The approximation of the interface modes $\boldsymbol{\Upsilon}_I(\boldsymbol{\theta}^k)$, at a sample point $\boldsymbol{\theta}^k$, is similar to the approximation scheme proposed for the fixed-interface normal modes. In this instance, the interface modes need to be computed at the support points $\boldsymbol{\theta}^l$, $l = 1,...,L$ and at the nominal point $\boldsymbol{\theta}^0$, that is, $\boldsymbol{\Upsilon}_I(\boldsymbol{\theta}^l), l = 0,1,...,L$.

3.5. Interpolation coefficients

The scheme suggested by (Goller et al. (2011)) and (Mayorga and Jensen (2018)) is considered in the present formulation for the purpose of obtaining the interpolation coefficients. First, the norm of the difference between the support points $\boldsymbol{\theta}^l, l = 1,...,L$ and the simulation point $\boldsymbol{\theta}^k$ is minimized, i.e.

$$\text{Min}_{l=1,...,L} \quad \| \boldsymbol{\theta}^l - \boldsymbol{\theta}^k \| \tag{10}$$

If the nearest point to $\boldsymbol{\theta}^k$ is denoted by $\boldsymbol{\theta}^q, q \in \{1,...,L\}$, the corresponding interpolation coefficient ξ_q^k is obtained by projecting $\boldsymbol{\theta}^k - \boldsymbol{\theta}^0$ onto $\boldsymbol{\theta}^q - \boldsymbol{\theta}^0$. The remaining part of the vector, that is, the component perpendicular to $\boldsymbol{\theta}^q - \boldsymbol{\theta}^0$ is represented as a linear combination of the remaining points $\boldsymbol{\theta}^l - \boldsymbol{\theta}^0, l = 1,...,L, l \neq q$. The coefficients of the linear combination are obtained by using the singular value decomposition (SVD) technique. The above interpolation scheme guarantees that the approximation is exact at each support point.

3.6. Parametrization of reduced-order matrices

Based on the previous approach and given the expansion of the substructure matrices $\mathbf{M}^s(\boldsymbol{\theta})$ and $\mathbf{M}^s(\boldsymbol{\theta})$ in (6), together with the approximation of the interface constraint modes $\boldsymbol{\Psi}_{ib}^s(\boldsymbol{\theta}^k)$ in (7), the approximation of the fixed interface normal modes $\boldsymbol{\Phi}_{id}^s(\boldsymbol{\theta}^k)$, and the approximation of the interface modes $\boldsymbol{\Upsilon}_I(\boldsymbol{\theta}^k)$, the reduced order matrices $\hat{\mathbf{M}}_{RI}$ and $\hat{\mathbf{K}}_{RI}$ in (5) can be evaluated directly at the sample point $\boldsymbol{\theta}^k$. Then, it is seen that the potential time-consuming step of computing the interface normal modes and the interface modes for different values of the model parameters has to be performed only for the support points. The accuracy of the approximations can be increased by densifying the region of interest in the model parameter space with additional support points.

4. EXAMPLE PROBLEM

4.1. Structural model

The three dimensional finite element building model shown in Figure 1 is considered for analysis. The model consists in a fifty four-story building model with a total height of 190.0 m. The building has a reinforced concrete core of shear walls and a reinforced concrete perimeter moment resisting frame. The columns of the perimeter have a circular cross section. The floors and shear walls are modeled by shell elements of different thicknesses τ. Additionally, beam and column elements are used in the finite element model which has 84244 degrees of freedom. Material properties are given by the Young's modulus $E = 2.77 \times 10^{10}$ N/m^2, mass density $\rho = 2,5 \times 10^3$ kg/m^3, and Poisson ratio $\mu = 0.3$. Finally, a 5% of critical damping is added to the model.

For an improved seismic performance, the structural system is reinforced with a total of 45 nonlinear vibration control devices. A typical configuration of these devices, at the floors where they are located, is shown in Fig.2. Each device consists of brace and plate elements where a series of metallic U-shaped flexural plates (UFP's) are located between the plates.

Each UFP exhibits a one-dimensional hysteretic type of non-linearity modeled by the restoring force law (Jensen and Sepulveda (2011))

$$f_{NL}(t) = \alpha\, k_e\, \delta(t) + (1-\alpha)\, k_e U^y\, y(t) \tag{11}$$

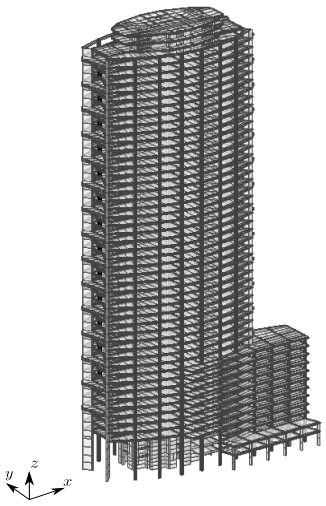

Figure 1: Three dimensional finite element building model.

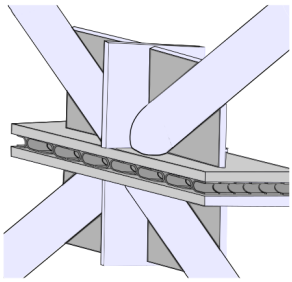

Figure 2: Model of vibration control device

where k_e is the pre-yield stiffness, U^y is the yield displacement, α is the factor which defines the extent to which the restoring force is linear, $y(t)$ is a dimensionless hysteretic variable, and $\delta(t)$ is the relative displacement between the upper and lower surfaces of the flexural plates. The hysteretic variable $y(t)$ satisfies the first-order non-linear differential equation

$$\dot{y}(t) = \dot{\delta}(t)\left[\beta_1 - y(t)^2[\beta_2 + \beta_3 \mathrm{sgn}(y(t)\dot{\delta}(t))]\right] \tag{12}$$

where β_1, β_2 and β_3 are dimensionless quantities that characterize the properties of the hysteretic behavior, $\mathrm{sgn}(\cdot)$ is the sign function, and all other terms have been previously defined. The following values for the dissipation model parameters are used in this case: $k_e = 2.5 \times 10^6$ N/m; $U^y = 1 \times 10^{-3}$m; $\alpha = 0.1$; $\beta_1 = 1.0$; $\beta_2 = 0.5$; and $\beta_3 = 0.5$. The non-linear restoring force of each device acts between the floors where it is placed along the same orientation of the device. For illustration purposes, a typical displacement-restoring force curve of one of the vibration control devices is shown in Figure 3.

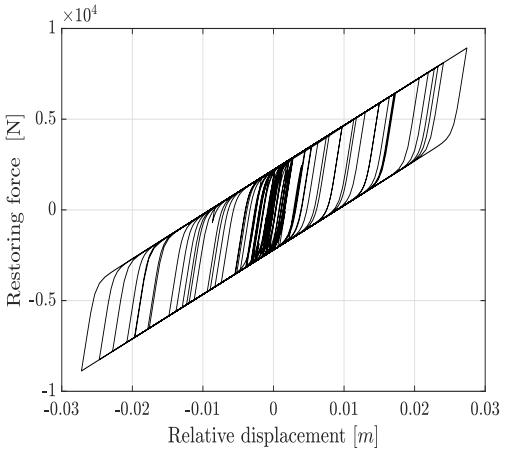

Figure 3: A typical hysteresis loop of the vibration control devices

4.2. Definition of substructures

The model is subdivided into 81 linear substructures $S_i, i = 1,...,81$ as shown in Figure 3. They are composed by three types of substructures, namely: core of shear walls located between two floors ($S_i, i = 1,...,27$); slabs of different floors ($S_i, i = 28,...,54$); and circular columns of the perimeter frame located between two floors and the corresponding slab of the intermediate floor ($S_i, i = 55,...,81$). In addition, there are 45 nonlinear substructures comprised by the nonlinear vibration control devices defined in the previous section. With this subdivision, the total number of internal degrees of freedom is equal to 60544, while 23700 degrees of freedom are present at the interfaces. A small number of fixed-interface normal modes are selected for the model. In particular, a model characterized by only 252 fixed-interface normal modes

is considered. In addition, 100 interface modes, which represent about 0.5% of the total number of interface degrees of freedom, are used in the reduced model. Thus, the total number of generalized coordinates of the reduced-order model represents a reduction of more than 99% with respect to the full finite element model.

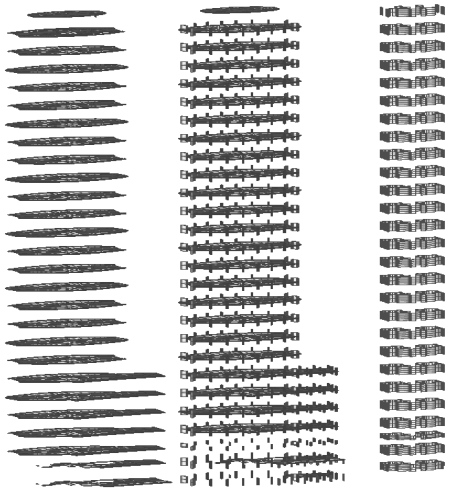

Figure 4: Substructures of the finite element model.

Validation calculations indicate that the reduced-order model is able to characterize accurately the important modes of the full finite element model.

4.3. Uncertainty propagation

The characterization of the system response requires system reanalyses as the finite element model changes due to variation in the values of the model parameters. Consequently, the reduced order matrices need to be re-computed for different values of the model parameters. In the framework of the present work, the required reanalyses are carried out by the parametrization scheme presented in Section 3.

It is assumed that the corresponding bending stiffness coefficient k_b and membrane stiffness coefficient k_m of the shell elements that model the core of shear walls are uncertain. The coefficient k_b is represented by the term $\tau^3 E$, while k_m is defined by the term τE. These coefficients are modeled as independent, discrete homogeneous isotropic Log-normal random fields (Chilès and Delfiner (1999)). Specifically, the random fields are discretized at six points along the height of the building. Each random field is characterized in terms of its mean value $\mu\mathbf{1}$, where $\mathbf{1}^T =< 1,1,1,1,1,1 >$, standard deviation σ, and correlation function $R(\Delta) = \exp(-\alpha\Delta^2)$, where the variable Δ represents a distance, and the parameter α is related to the correlation length of the random field. The corresponding covariance matrix of each one of the discrete random fields is given by $\mathbf{\Sigma} = \sigma^2\mathbf{R}$, where $\mathbf{R}$ is the correlation matrix with coefficients $\mathbf{R}_{ij} = R(\Delta_{ij}), i,j = 1,...,6$, where Δ_{ij} is the distance between the different points of the discretized random field. For instance, the discrete Log-normal random field $\mathbf{k}_b$ can be expressed as

$$\mathbf{k}_b = \exp(\mu_N\mathbf{1} + \mathbf{\Phi}\mathbf{\Lambda}^{1/2}\mathbf{y}) \tag{13}$$

where $\mu_N\mathbf{1}$ represents the mean value of the corresponding underlying Gaussian random field that characterized the discrete Log-normal random field, $\mathbf{\Phi}$ and $\mathbf{\Lambda}$ correspond to the spectral decomposition of the covariance matrix of the underlying Gaussian random field $\mathbf{\Sigma}_N$, and $\mathbf{y}$ is a vector of independent standard normal random variables (Der Kiureghian (2004)). A similar representation allows the discrete Log-normal random field $\mathbf{k}_m$. The mean values of the random fields are set equal to $\mu_{k_b} = 5.98 \times 10^9$ N/m^2 and $\mu_{k_m} = 1.66 \times 10^{10}$ N/m^2, respectively, with a coefficient of variation equal to 15%. A medium correlated random field is considered by selecting an appropriate value of α. With respect to Section 3 and based on the previous characterization of the uncertain parameters, it is clear that substructures $S_i, i = 1,...,27$ depend on the model parameters while the rest of the substructures are independent of such parameters. Note that the model parameters correspond to the components of the discrete random fields $\mathbf{k}_b$ and $\mathbf{k}_m$. The parametrization functions of the substructure matrices associated with a particular component of the discrete random field $\mathbf{k}_b$ or $\mathbf{k}_m$, say θ_j, are given by $h_j(\theta_j) = \theta_j$ and $g_j(\theta_j) = 1, j = 1,...,6$, where the model parameter is given by $\theta_j = \tau^3 E$ or $\theta_j = \tau E$.

For illustration purposes, the structural response

to be controlled is the displacement at the top of the building. The model is excited by a ground acceleration generated by a source-based model derived in terms of Green's functions and strong pulse-motion generation areas (SPGA) (Nozu et al. (2014)). Such model has reproduced successfully acceleration and velocity records from mega-thrust earthquakes. The sampling interval and the duration of the excitation are taken equal to $\Delta t = 0.01$ s and $T = 50$ s, respectively. The synthetic ground acceleration used in the present uncertainty propagation analysis is shown in Fig. 5.

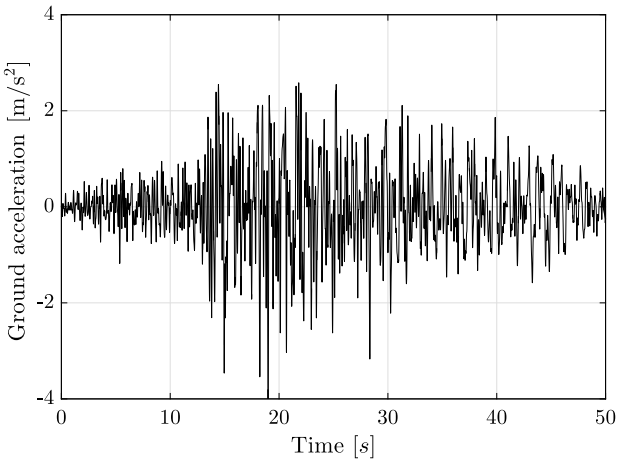

Figure 5: Synthetic ground acceleration sample based on a source-based model for subduction mega-thrust earthquakes

Due to page limitations, the description, characterization and implementation of a fully stochastic excitation model derived from the SPGA method is not considered in this work. Only the effect of uncertain structural model parameters is taken into account for the uncertainty analysis. Information about the SPGA stochastic excitation model can be found in (Jerez et al. (2017)).

4.4. Results

The histograms of the displacement at the top of the building based on 2000 simulations obtained with the full finite element model and the reduced-order model are shown in Figs. 6 and 7. The number of support points in the parameter space used in the proposed parametrization scheme is equal to 24. The generation of such points is based on the Latin Hypercube sampling method.

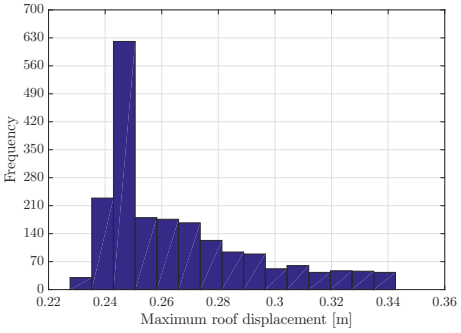

Figure 6: Histogram of maximum roof displacement. Full model

Table 1: Statistics of maximum roof displacement. FM: full finite element model, ROM: reduced-order model

Model	Mean [m]	Standard deviation [m]
FM	0.265	0.0267
ROM	0.266	0.0269

It is seen that the histograms are very similar. Some statistics of the histograms are provided in Table 1. The comparison of the results obtained with the reduced order model shows an excellent correspondence with the unreduced model. In terms of computational effort, the execution time for obtaining the previous results using the reduced-order model is decreased by a factor of more than 5 with respect to the case when the full finite element model is used. This significant reduction in computational effort is achieved without compromising the accuracy of the results.

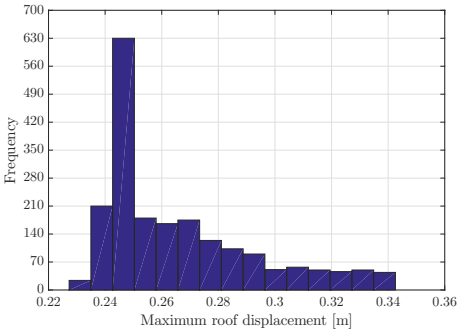

Figure 7: Histogram of maximum roof displacement. Reduced-order model

5. CONCLUSIONS

A parametric substructure approach in the context of uncertainty propagation of stochastic dy-

namical systems has been presented. The substructures internal dynamic behavior is described by a set of dominant fixed interface normal modes. On the other hand, interface reduction is achieved by considering a reduced number of interface modes. In this manner, accurate and highly reduced-order models of complex finite element models are obtained. The proposed method has been validated in a complex nonlinear finite element model under a ground acceleration generated by a realistic source-based model. Validation calculations show that an important reduction in computational effort can be achieved without compromising the accuracy of the results. Future research efforts involve the consideration of a fully stochastic excitation model in the context of uncertainty propagation. In this manner, the effect of uncertain structural model parameters as well as the stochastic nature of the excitation can be considered explicitly in the analysis.

6. ACKNOWLEDGMENTS

The research reported here was supported in part by CONICYT (National Commission for Scientific and Technological Research) under grant number 1150009. Also, this research has been implemented under the PAC (Programa Asistente Cientifico 2017)-UTFSM program. These supports are gratefully acknowledged by the authors.

7. REFERENCES

Castanier, M., Tan, Y., and Pierre, C. (2001). "Characteristic constraint modes for component mode synthesis." *AIAA Journal*, 39(6), 1182–1186.

Chilès, J. and Delfiner, P. (1999). "Geostatistics: modeling spatial uncertainty." *Wiley, New York*.

Craig, R. (1981). "Structural dynamics, an introduction to computer methods." *John Wiley and Sons*.

Der Kiureghian, A. (2004). "Engineering design reliability handbook." *CRC Press*.

Goller, B., Pradlwarter, H., and Schuëller, G. (2011). "An interpolation scheme for the approximation of dynamical systems." *Computer Methods in Applied Mechanics and Engineering*, 200, 414–423.

Jensen, H., Araya, V., Muñoz, A., and Valdebenito, M. (2017). "A physical domain-based substructuring as a framework for dynamic modeling and reanalysis of systems." *Computer Methods in Applied Mechanics and Engineering*, 326, 656–678.

Jensen, H. and Sepulveda, J. (2011). "On the reliability-based design of structures including passive energy dissipation systems." *Structural Safety*, 34, 390–400.

Jerez, D., Jensen, H., and Nozu, A. (2017). "Development of a stochastic model for the generation of seismic excitation and its application to reliability analysis." *Proceedings Jornadas Mecanica Computacional, La Serena, Chile, 9-11 October*, 1.

Mayorga, F. and Jensen, H. (2018). "An interpolation scheme for estimating modal information of reduced-order models: application to uncertainty propagation." *Proceedings Jornadas Mecanica Computacional, Punta Arenas, Chile, 9-11 October*, 1.

Nozu, A., Yamada, M., Nagao, T., and Irikura, K. (2014). "Generation of strong motion pulses during huge subduction earthquakes and scaling of their generation areas." *Journal of Japan Association for Earthquake Engineering*, 14(6), 96–117.

Papadimitriou, C. and Papadioti, D. (2013). "Component mode synthesis techniques for finite element model updating." *Computers and Structures*, 126, 15–28.

Seidel, R. (1997). "Handbook of discrete and computational geometry. convex hull computations, ch. 19." *CRC Press*.